Available online at www.sciencedirect.com
SCIENCE DIRECT®
Journal of Catalysis 231 (2005) 430–437
JOURNAL OF CATALYSIS
www.elsevier.com/locate/jcat

Selective oxidation of methane over $Sn_{1-x}Ge_xO_2$

Kenji Tabata [a,*], Takashi Kawabe [b], Yoichi Yamaguchi [c], Eiji Suzuki [d], Tatsuaki Yashima [a,1]

[a] *Research Institute of Innovative Technology for the Earth (RITE) 9-2, Kizugawa-dai, Kizu-cho, Soraku-gun, Kyoto 619-0237, Japan*
[b] *Technology Research Laboratory, Shimadzu Corporation, 3-9-4, Hikaridai, Seika-cho, Soraku-gun, Kyoto 619-0237, Japan*
[c] *Nano-Instrument Technology Unit, Nano-Materials Research Laboratory, KRI Inc., Kyoto Research Park, 134, Chudoji Minami-machi, Shimogyo-ku, Kyoto 600-8813, Japan*
[d] *Department of Fine Materials Engineering, Shinshu University 3-15-1, Tokida, Ueda 386-8567, Japan*

Available online 23 March 2005

Abstract

The effects of germanium ion incorporation into tin oxide on the selectivity for the selective oxidation of methane in the presence of NO over $Sn_{1-x}Ge_xO_2$ ($x = 0$–0.5) were examined with the use of a conventional catalytic reaction and theoretical calculations. The reactivity of the tin oxide for methane oxidation was decreased by the incorporation of germanium. The product selectivity was measured at 10% methane conversion. The product was CO_2, CO, and a small amount of C_2 compounds in the absence of germanium, but we obtained C_1-oxygenates over every germanium ion-incorporating catalyst. The main product of the C_1-oxygenates was formaldehyde. The selectivity of formaldehyde increased with the content of germanium (x) and had a maximum value at $x = 0.2$. We considered two reaction routes of HCHO formation: a heterogeneous reaction and a homogeneous one. Since a larger proportion of CO_2 selectivity in comparison with CO selectivity was found in the presence of $Sn_{0.9}Ge_{0.1}O_2$, we assumed that the heterogeneous reactions over the catalyst were dominant in a lower temperature region below ca. 860 K. We suggested that the C_1-oxygenates were produced on the $Sn_{0.9}Ge_{0.1}O_2$ catalyst, not in the gas phase. We theoretically predicted that the substituted germanium ion occupied the site for fourfold Sn^{2+} on the topmost layer by the DFT theoretical calculations. From the results of calculation, we assumed that the coverage of chemisorbed oxygen on the Ge/SnO_2 (110) surface was expected to be smaller than that on the SnO_2 (110) surface through the reactions, and we concluded that the smaller amount of chemisorbed oxygen through the reactions and the obstruction of oxygen migration over the Ge/SnO_2 was favorable to an increase in the selectivity for C_1-oxygenates in the reaction.

Keywords: Selective oxidation; Mathane; SnO_2; Theoretical calculation

1. Introduction

Direct conversion of methane with oxygen into C_1-oxygenates (formaldehyde and methanol) is a potentially important process, not only for the effective use of natural gas resources, but also for minimization of energy consumption. Various research studies on noncatalytic or catalytic oxidation of methane to the oxygenates have been carried out since the early 1900s, but the reported yields of C_1-oxygenates have not come up to the level required to substitute for the current energy-consuming process from the syngas that was formed from methane by steam reforming [1–4].

The rate-determining step of the selective oxidation of methane is the abstraction of the first hydrogen atom from CH_4, and this large value of the dissociation energy brings about the sequential oxidations to easily produce carbon mono- and dioxides. To circumvent the deep oxidations, very-low-area catalysts [5] or very-low-loading M/SiO_2 (M = Fe, V, Bi) catalysts [6] were examined with and without radical generative additives such as NO. These trials were intended to increase the conversion of methane and

* Corresponding author. Fax: +81 985 58 7323.
E-mail address: kenjt@cc.miyazaki-u.ac.jp (K. Tabata).
[1] Present address: Department of Applied Chemistry, Faculty of Engineering, Miyazaki University 1-1, Gakuen-Kibanadai, Miyazaki-City, Miyazaki, 889-2192, Japan.

0021-9517/$ – see front matter
doi:10.1016/j.jcat.2005.02.008

to prevent deep oxidation of the C_1-oxygenates. Nitrogen oxides (NO_x) have also been used to promote gas-phase reactions [4,5,7–9]. The precise mechanisms of these combined gas-phase reactions and catalytic reactions have not been clarified.

There are several approaches to the design of effective catalysts for methane selective oxidation [10–15]. Taylor et al. reported that a successful methane selective oxidation catalyst must: (i) not destroy the desired product such as methanol; (ii) activate methane; and (iii) activate oxygen [15]. The utilization of a highly reactive oxygen species over a catalyst has been examined. Liu et al. reported that a highly reactive O^- species was generated after the interaction of N_2O with the surface of MoO_3 supported on Cab–O– Sil M-5 silica [16]. They concluded that the reactive O^- species was responsible for the initiation of CH_4 conversion.

We have studied the interaction of oxygen with a reduced SnO_2 thin film with X-ray photoelectron spectroscopy (XPS) [17,18]. Four kinds of chemisorbed oxygen species (O_b, O^-, O_2^{2-}, O_2^-) were observed after O_2 exposure at room temperature on the reduced SnO_2 thin film [18]. We theoretically studied the interaction of oxygen with the reduced SnO_2 (110) surface by the density functional theory (DFT) [19]. In that paper, we predicted the presence of two kinds of chemisorbed oxygen species (O_2^{2-}, O_2^-) on the surface and the presence of O^- that had the oxygen vacancy at the nearest-neighboring site. O_b was suggested to be O^{2-} ion at the bridging site on the topmost layer of the SnO_2 (110) surface without oxygen vacancies around it [18].

Recently we succeeded in synthesizing a rutile-type germanium-incorporated tin oxide [20]. It is expected that the properties of surface oxygen species could change with the replacement of tin atoms with germanium atoms; that is, it is the same IVB group metal, its ionic crystal radius is smaller than that of tin, and its electronegativity is higher than that of tin. The rutile-type germanium-incorporated tin oxide is therefore expected to show the different interaction of oxygen on the surface, and this variation would affect the selectivity of C_1-oxygenates in the methane oxidation.

In this paper, we examine the effects of germanium addition to SnO_2 on the activities and the selectivities for the selective oxidation of methane in the presence of NO. A theoretical approach to the catalytic properties of those oxides for the methane selective oxidation is also discussed.

2. Experimental

2.1. Catalyst preparation

The details of the preparation procedures for $Sn_{1-x}Ge_xO_2$ ($x = 0$–0.5) appear in our previous paper [20]. In this study, we utilized commercially obtained $Sn(i\text{-}OC_3H_7)_4$ and $Ge(OC_2H_5)_4$, and $i\text{-}C_3H_7OH$ was used as a solvent. All of the procedures gave a hard xerogel and were the same as our previous ones. The hard xerogel was ground to a fine powder and then calcined at 973 K under air for 24 h. We measured X-ray diffraction patterns of $Sn_{1-x}Ge_xO_2$ (RINT 2000, Rigaku). BET surface areas were measured on Autosorb-1 (Quanta Chrome Co.).

2.2. CH_4–O_2–NO reaction

Highly purified methane (> 99.9995%), oxygen (> 99.9999%), and helium (> 99.9999%) and 3.0 mol% NO (He balance) were used. The standard gas composition (CH_4, 55.5 mol%; O_2, 27.8 mol%; NO, 0.5 mol%; He, balance) was controlled with a mass flow controller. The feed gas was mixed just before the inlet of the reactor. All of the experiments were carried out with a conventional flow reactor system. A quartz-glass tubing reactor (7 mm i.d.) was heated with an electric furnace. The length of the heating zone was 100 mm. The temperature of the reaction was measured with a thermocouple attached to the outside wall of the reactor tube at the center of the heating zone.

The catalysts were fixed with quartz-glass wool at the center of the reactor. The weight of every catalyst was 0.05 g. The feed gas was supplied from the top of the reactor and was controlled at 240 ml min^{-1}. Methane conversion was measured as a function of reaction temperatures. Products were analyzed with two on-line gas chromatographs. Carbon monoxide, carbon dioxide, ethane, ethene, formaldehyde, methanol, and nitromethane were detected with a FID (Gaskuropack 54) and a methanizer. For methane and oxygen, an activated carbon column and TCD were also used. The carbon balance was over 95%. All gas lines from the exit of the reactor to the gas chromatograph were heated at 393 K to avoid condensation of oxygenates and water. Data shown in this paper were obtained at 30 min or more after the beginning of the reaction. All experiments were repeated at least three times.

2.3. DFT calculation method

All of the density functional theory (DFT) calculations were performed in the framework of commercial software, the DMol^3 package of programs [21]. All electrons were treated in the geometrical optimization for the adsorbed oxygen species on the monolayer reduced Ge/SnO_2 (110) cluster within the generalized gradient approximation (GGA) level of theory, with the use of Becke–Lee–Yang–Parr nonlocal type functional (BLYP) [22]. The correction of the relativistic effects of the heavy atoms Ge and Sn were also considered. The geometries of the clusters were fixed at a SnO_2 crystal [23]. The vibrational frequencies of the adsorbed O_2 molecule and the transition state for its dissociation on the monolayer clusters were also calculated at the same level of theory. Also based on the optimal structures, single-point energies for the three-layer reduced Ge/SnO_2 (110) clusters with oxygen were calculated with the effective core potential (ECP) and GGA-BLYP levels of theory. A Fermi surface thermal smearing parameter of 0.02 atomic units was

Table 1
Specific surface area (m^2/g) of $Sn_{1-x}Ge_xO_2$ and their onset temperatures (K) of significant CH_4 conversion

$Sn_{1-x}Ge_xO_2$	Specific surface area	Onset temperatures of significant CH_4 conversion
$x = 0$	20.3	ca. 690
$x = 0.05$	32.1	ca. 820
$x = 0.1$	26.7	ca. 840
$x = 0.14$	28.8	ca. 860
$x = 0.2$	29.1	ca. 860

used to arrive at a self-consistent field (SCF) convergence of the present calculations. The basis sets used throughout were the standard double numerical atomic basis sets plus d-functions (DND). The Madelung potential is not applied to the present calculations, though we have determined that the Coulomb interaction from the outside of the cluster is significantly weakened by the screening effect. The mono- and three-layer reduced Ge/SnO_2 clusters were, respectively, C_{2v}: $Sn_8Ge_2O_{15}$ (the area in the dotted lines) and D_{2h}: $Sn_{27}Ge_4O_{50}$, as shown in Fig. 7b. Because the incorporation of Ge at site B on the Ge/SnO_2 surface provides the most stable structures (see Table 1), we modeled the reduced mono- and three-layer clusters with the two and four Ge atoms substituted for Sn atoms in the symmetrical equivalent site B, respectively. The clusters are electrically neutral species. Although there is a lack of information on the adsorption sites of the O_2 molecule on a reduced Ge/SnO_2 and SnO_2 (110) surface, we assume that it adsorbs at a vacant bridging oxygen site on each surface, as on the TiO_2 (110) surface [24]. We doubt the validity of the distribution of the spin densities of the cluster with the open-shell oxygen species because the present DFT level of the unrestricted GGA calculations indicates that the spin densities exist predominantly in the reduced clusters, not in the adsorbed O_2^- species. Therefore, we set the singlet spin state for all of the present clusters with oxygen.

We also calculated the adsorption energies for CH_3OH, CH_3O, CH_2O, OH, and H_2O produced by the methane oxidative reactions on the above monolayer reduced Ge/SnO_2 cluster. The oxygen atoms of adsorbates exist at the topmost bridging oxygen vacant site between the fourfold Ge^{2+} ions of the cluster. The geometries of adsorbates were optimized under the condition of fixed geometries of the clusters, with the use of the effective core potential (ECP) and GGA-BLYP levels of theory. Similar DFT calculations have been made for the adsorbates on the reduced SnO_2 (110) surfaces for comparison. A Silicon Graphics Origin 2000 R10000 workstation was used for the present calculations.

3. Results and discussion

3.1. Reactivity and selectivity of $Sn_{1-x}Ge_xO_2$

The X-ray diffraction patterns of $Sn_{1-x}Ge_xO_2$ ($x = 0$–0.5) were recorded. All of the diffraction patterns obtained for the specimens were fully explained to be identical to a tetragonally crystallized SnO_2, cassiterite [25], and space group $P4_2/mnm$ [26]. This means that Sn atoms of SnO_2 are partially replaced by Ge atoms of the added GeO_2.

Methane conversions over SnO_2 and the Ge-incorporated SnO_2 in CH_4–O_2–NO are shown in Fig. 1. The conversion of methane over SnO_2 rapidly increased around 690 K. The conversions were lowered by the addition of germanium in a lower temperature region. The conversions of methane over the $Sn_{1-x}Ge_xO_2$ ($x = 0.05$–0.2) were raised clearly around 870 K. We compared the onset temperatures of significant CH_4 conversion of these samples and their specific surface areas as shown in Table 2. All of the values of specific surface area are in the region of 20–32 m^2/g. All of the onset temperatures were above 820 K, but $Sn_{0.9}Ge_{0.1}O_2$ had another onset point of CH_4 conversion at ca. 660 K. We also showed the conversion of methane in the absence of a catalyst in Fig. 1. The onset temperature of CH_4 conversion in the absence of catalyst was ca. 840 K, and this temperature is very close to those observed in the presence of $Sn_{1-x}Ge_xO_2$ catalyst.

We studied also the variation of selectivities of the products over $Sn_{0.9}Ge_{0.1}O_2$ in the reaction temperatures between 573 K and 923 K as shown in Figs. 2 and 3. A marked vari-

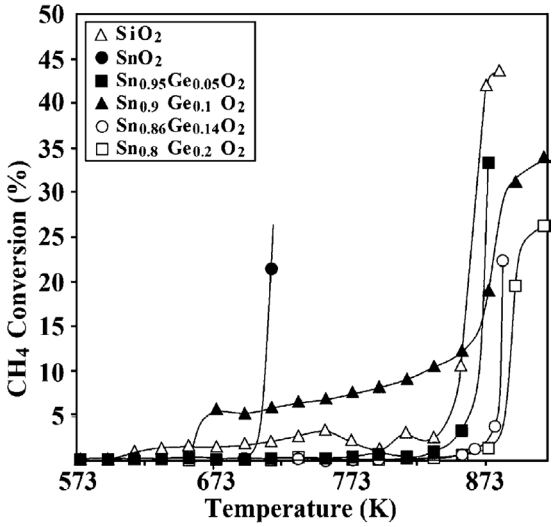

Fig. 1. CH_4 conversion as a function of reaction temperatures. CH_4/O_2, 0.5; NO concentration, 0.5%; catalyst weight, 0.05 g; SV = 3740 h^{-1}.

Table 2
Relative energies (RE, kcal/mol) and net charges (NC, |e|) at each substitute site[a] of a Ge atom for an Sn atom in the three-layer stoichiometric and reduced SnO_2 cluster

Atom	Site	Stoichiometric cluster		Reduced cluster	
		RE	NC	RE	NC
Ge(Sn)	A	0.0	+1.14 (+1.90)	0.0	+1.14 (+1.89)
	B	−5.2	+1.09 (+1.78)	−14.4	+0.69 (+1.19)
	C	−0.7	+0.98 (+1.54)	−3.2	+0.91 (+1.47)

Values in parentheses are for the Sn atom at each site before the substitution.
[a] Defined in Fig. 7.

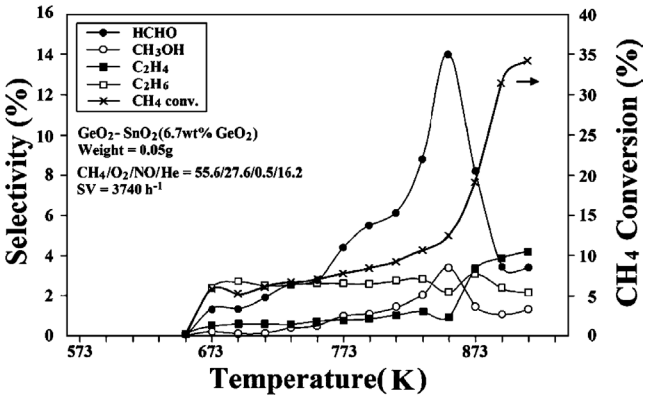

Fig. 2. Selectivity of C_1-oxygenates and C_2-compounds to products for $Sn_{0.9}Ge_{0.1}O_2$ as a function of reaction temperatures. Reaction condition was the same as shown in Fig. 1.

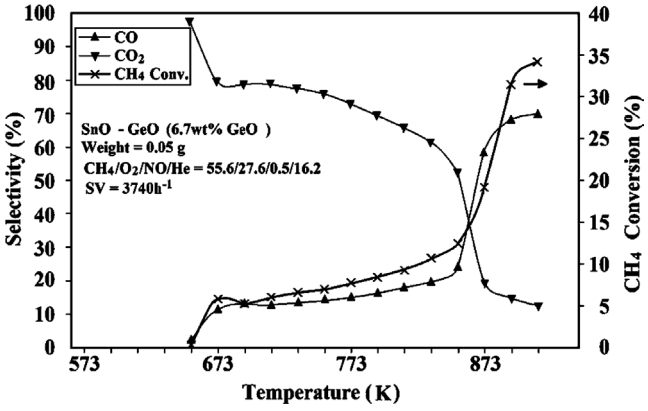

Fig. 3. Selectivity of CO and CO_2 to products for $Sn_{0.9}Ge_{0.1}O_2$ as a function of reaction temperatures. Reaction condition was the same as shown in Fig. 1.

ation in Fig. 2 is that of HCHO selectivity. Its selectivity gradually increased in a lower temperature region and then increased rapidly from around 810 K. The HCHO selectivity had a peak at ca. 840 K and then decreased rapidly. The variation of CH_3OH is similar to that of HCHO but smaller than that of HCHO. The proportions of C_2H_4 and C_2H_6 were also small.

The selectivity for CO_2 varied largely as opposed to that for CO in the measured reaction temperature region (Fig. 3). The selectivity for CO_2 decreased largely from around 850 K. On the other hand, that for CO increased largely from around that temperature. The peak point of HCHO selectivity is close to that temperature.

Each selectivity proportion of the products to the contents of Ge in SnO_2, that is, C_1-oxygenates, C_2 species, CO, CO_2, and CH_3NO_2, at 10% methane conversion is shown in Fig. 4. The reaction temperatures also at 10% methane conversion are shown in Fig. 4. In the absence of germanium, the main product was CO_2. The selectivity for CO_2 exceeded 80%. A smaller proportion of CO and a trace of C_2 species were observed in the products of SnO_2. C_1-oxygenates were not observed in the products.

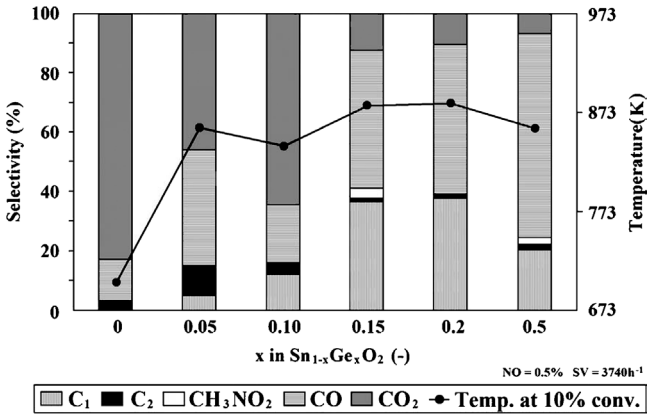

Fig. 4. Selectivity to products as a function of x in $Sn_{1-x}Ge_xO_2$ and reaction temperatures at 10% CH_4 conversion. Reaction condition was the same as shown in Fig. 1.

In all of the germanium-incorporated samples from $x = 0.05$ to 0.5 of $Sn_{1-x}Ge_xO_2$, C_1-oxygenates was observed to a greater or lesser extent. The main component of the C_1-oxygenates was HCHO, as shown the selectivity variation in Fig. 2. The selectivity for C_1-oxygenates increased gradually with the value of x; it reached a peak at $x = 0.2$ and then decreased slightly. The selectivity for CO was increased by the germanium incorporation, but that of CO_2 decreased largely in the region of $x \geqslant 0.14$. The selectivity for CO at 10% CH_4 conversion was 33.6% in the absence of catalyst. That for CO_2 was 0% at the same CH_4 conversion. From the opposed variations between CO_2 and CO proportions in Fig. 4 and the variation of CH_4 conversion in the presence of SiO_2, we determined that the contribution from the homogeneous reactions in the reaction gradually increased in the region of $x \geqslant 0.14$ [4]. We also determined the contribution from the heterogeneous reactions, especially for $Sn_{0.9}Ge_{0.1}O_2$, to the production of C_1-oxygenates in a lower temperature region.

3.2. Effects of NO addition on the selectivities

Bañares et al. reported that the addition of NO for the selective oxidation of CH_4–O_2 over V_2O_5/SiO_2 increased the conversion of methane and showed a strong effect on their product distribution [5]. We also examined the effects of NO addition on the conversion of methane and the selectivities of products for the selective oxidation of methane over $Sn_{0.8}Ge_{0.2}O_2$, as shown in Figs. 5 and 6. The conversion of methane increased largely with the addition of a small amount of NO to the reaction gas, and then the enhancement of that was small with the further addition of NO as shown in Fig. 5. This result over $Sn_{0.8}Ge_{0.2}O_2$ was very similar to that over V_2O_5/SiO_2 [5].

Fig. 6 shows the selectivity variations of HCHO, CH_3OH, CO, and CO_2 with NO concentration at 10% methane conversion. The conversion of methane over $Sn_{0.8}Ge_{0.2}O_2$ in the absence of NO was lower than 10% through the examined reaction temperature region. The selectivity variation of HCHO inversely related to that of CO, but it was hard to ex-

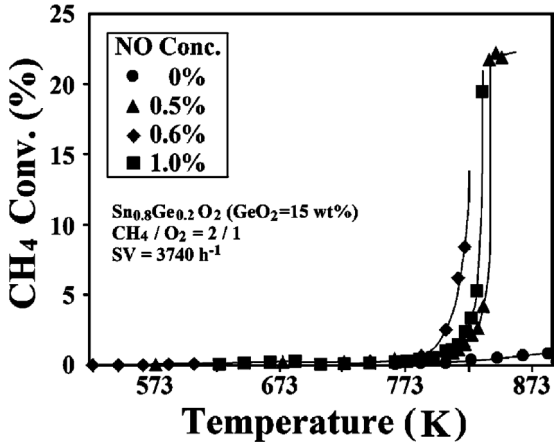

Fig. 5. Effects of NO concentration on CH_4 conversion for $Sn_{0.8}Ge_{0.2}O_2$ as a function of reaction temperatures. Reaction condition was the same as shown in Fig. 1.

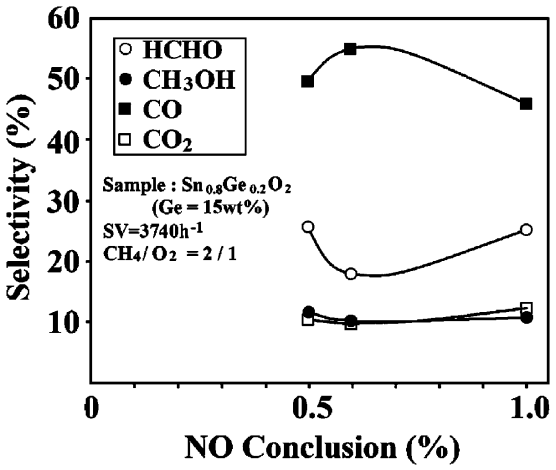

Fig. 6. Selectivity to products as a function of NO concentration at 10% CH_4 conversion. Any other reaction condition except for NO concentration was the same as shown in Fig. 1.

plain clearly by the effects of NO addition. The selectivities for CH_3OH and CO_2 hardly changed through the variation of NO concentration. We therefore assumed that the addition of NO to the reaction gas did not have a strong effect on the yield of the C_1-oxygenates over $Sn_{1-x}Ge_xO_2$.

3.3. Calculated results for the incorporated site of germanium ion

Since the enhancement of C_1-oxygenate selectivity was obtained in the presence of $Sn_{0.9}Ge_{0.1}O_2$ in a lower temperature region, we tried to clarify the reason. First, we studied a feasible site of incorporated Ge ion. To investigate the incorporated site of Ge ion in a SnO_2 crystal with the rutile structure, we examined theoretically the energetic stability and Mulliken atomic net charges of alternative substitution sites for a Ge ion replacing an Sn ion, with the use of the three-layer stoichiometric cluster, $Sn_{30}GeO_{56}$, and the reduced cluster, $Sn_{30}GeO_{50}$ (see Figs. 7a and b, respectively), as in a previous study [19b]. The results of the single point energies at the GGA level for these clusters are summarized in Table 2; here the substitution sites are defined in Fig. 7. The energy of the sixfold coordinated Ge^{4+} at site A in the second layer of each cluster is taken as a reference. We found that both the stoichiometric and the reduced Ge/SnO_2 surfaces provided the most stable structures when the Ge ions were incorporated at the sixfold coordinated Sn^{4+} on the topmost layer (B site).

There is a larger change in the Mulliken atomic net charge of germanium at site B between the stoichiometric cluster and the reduced one in comparison with the cases at every site of A and C as shown in Table 2. The smaller value of positive net charge of germanium at the fourfold coordinated site B of the reduced surface shows a larger ability to interact with oxygen molecules.

It is noted that because the oxide catalysts were prepared under oxidative conditions to yield smaller oxygen defects, we expect to obtain a stoichiometric Ge/SnO_2 catalyst with the sixfold coordinated Ge^{4+} at site B. We expected to find

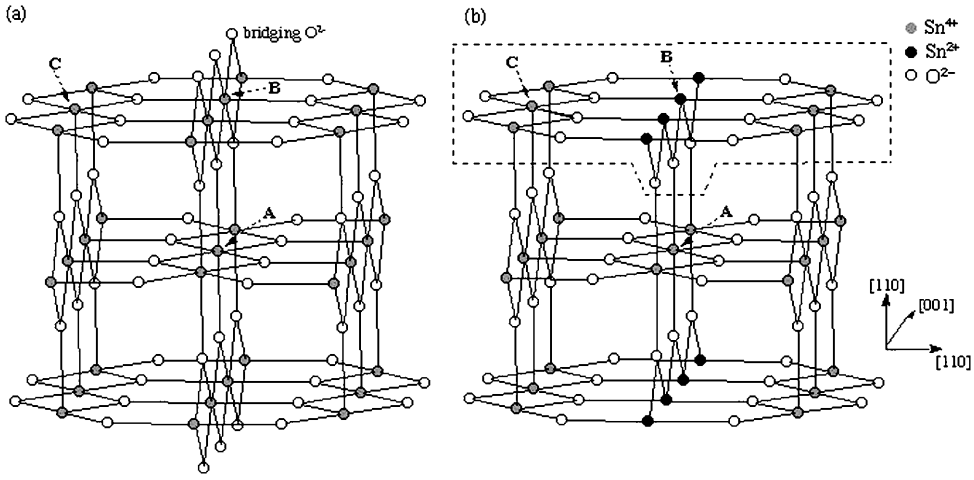

Fig. 7. Schematic three-layer structures for the stoichiometric (a) and the reduced (b) SnO_2 (110) clusters. The substitution sites (A, B, and C) of Ge atom on the model are shown in the figure.

that the random substitution of Ge for Sn at site B occurred, which produced the formation of a Ge^{4+}–O–Sn^{4+} bridging bond in the Sn^{4+}–O–Sn^{4+} bridging bond.

3.4. Calculated results of oxygen interaction

The calculated results for the two types of O_2 molecule adsorptions are summarized in Table 3: the side-on type in which O_2 lies flat on the (110) surface and the end-on type where O_2 stands straight on the (110) surface. We assigned the molecularly chemisorbed oxygen species at the end-on type and the side-on type on the reduced SnO_2 surface to the superoxo (O_2^-) and peroxo (O_2^{2-}) from a comparison of the calculated results and the experimental results of the bond lengths of O–O and the vibrational frequencies [19]. The calculated adsorption energy of the O_2 molecule at the side-on type was larger than that of the O_2 molecule at the end-on type. A potential energy diagram of the adsorption, dissociation, and migration of oxygen on the reduced (110) surface appears in Fig. 8. The total energies of the separated $^3O_2$ molecule and the three-layer reduced SnO_2 cluster were taken as a reference. The top view of the clusters with the adsorbed oxygen species is also shown as an inset in Fig. 8. We predicted a small dissociation energy of 2.0 kcal/mol for the O_2 molecule at the transition state (TS) on the three-layer cluster model of SnO_2. The migration barriers of an oxygen atom were calculated from PS1 to PS4. The oxygen atom was stabilized at the vacant bridging oxygen site in PS1 and PS3 and destabilized above the Sn^{2+} site in PS2 and above Sn^{4+} site in PS4. The migration barriers of the oxygen atom on the three-layer cluster of SnO_2 between PS1 and PS3 were predicted to be 16.9–17.5 kcal/mol. The energy difference of 13.0 kcal/mol between PS3 and PS4 corresponds to the migration barrier of the oxygen atom to the nearest neighboring row of Sn^{4+}.

Table 3
Calculated results for the adsorbed O_2 molecules on the mono- and three-layer reduced Ge/SnO_2 and SnO_2 (110) clusters

	Ge/SnO_2 (110)			SnO_2 (110)[c]		
	End-on	Side-on	TS[d]	End-on	Side-on	TS[d]
Bond lengths[a], O–O (Å)	1.312	1.442	1.645	1.347	1.435	1.909
Vibrational frequencies, ν(O–O)(cm^{-1})	1005	674	504i	968	718	661i
Adsorption energies[b], (kcal/mol)	11.8	17.5	17.6	16.5	25.7	23.7
Assignment of adsorbed O_2 species	O_2^-	O_2^{2-}		O_2^-	O_2^{2-}	

[a] Monolayer model.
[b] Three-layer model.
[c] Ref. [23].
[d] Transition state for the dissociation of the side-on type adsorbed O_2 molecule.

The interaction of oxygen with the reduced Ge/SnO_2 cluster was similarly simulated. Two Sn^{2+} ions at the four-fold coordinated site of the topmost layer of the SnO_2 cluster model were replaced with two Ge^{2+} ions. The molecularly chemisorbed oxygen species at the end-on type and the side-on type on the reduced Ge/SnO_2 surface were also assigned to the superoxo (O_2^-) and peroxo (O_2^{2-}). Both the calculated adsorption energies of O_2 molecule for the Ge/SnO_2 cluster model at the end-on type and side-on type were smaller than those for the SnO_2 cluster model. The lowering of stability of the adsorbed O_2 molecule on the Ge/SnO_2 was suggested. A potential energy diagram for the adsorption, dissociation (TS), and migration of oxygen on the reduced Ge/SnO_2 surface is also shown in Fig. 8.

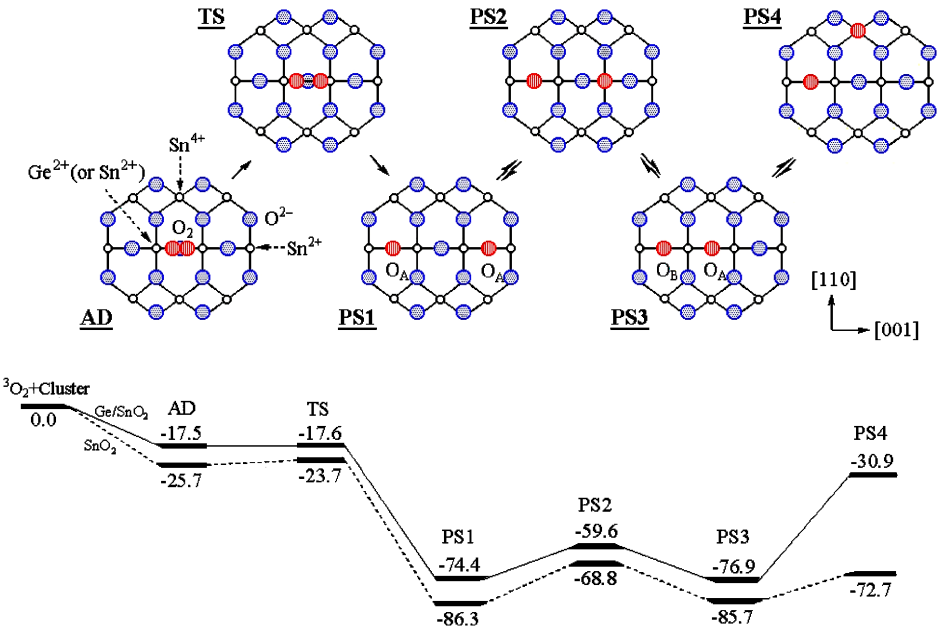

Fig. 8. Calculated potential energy diagram for adsorption (AD), dissociation (TS), and migration (PS1–PS4) of oxygen on the three-layer reduced SnO_2 and Ge/SnO_2 clusters. Relative energies are given in kcal/mol. The top view of the clusters with oxygen species is shown.

The dissociation energy of the O_2 molecule on the reduced Ge/SnO_2 cluster was close to zero. The migration barriers of the oxygen atom on the reduced (110) surface of the Ge/SnO_2 cluster between PS1 and PS3 were predicted to be 14.8–17.3 kcal/mol. These values were similar to those on the reduced SnO_2 cluster. The migration barrier of the oxygen atom between PS3 and PS4 corresponds to the migration barrier of the oxygen atom to the nearest neighboring row of the fivefold coordinated Sn^{4+}. It was calculated to be 46.0 kcal/mol. Thus, it is most unlikely that an adsorbed oxygen atom can migrate from the bridging oxygen site to the fivefold coordinated Sn^{4+} site on the reduced Ge/SnO_2 cluster model.

3.5. Calculated adsorption energy

The methyl group, methoxide, CH_3OH, and CH_2O_2 were observed in the C 1*s* level spectra of XPS for the SnO_2 thin film after methane exposure at 473 K in our previous study [27]. We calculated that the adsorption energies of CH_3OH, CH_3O, CH_2O, CH_2O_2, OH, and H_2O on the monolayer reduced both the SnO_2 and the Ge/SnO_2 cluster models with the DFT calculation method. The adsorption energies were calculated on both the fivefold Sn^{4+} site and the fourfold Sn^{2+} site on the cluster models. The calculated adsorption energy and net charge of each adsorbate are summarized in Table 4. For comparison, the calculated results for the case of the reduced SnO_2 (110) surface are also added in Table 4, for the case where the oxygen atoms of the adsorbates are bound to the fivefold Sn^{4+} or exist at the topmost bridging oxygen vacant site. CH_3OH and CH_2O were predicted not to stabilize on both the fourfold Sn^{2+} site on the SnO_2 cluster model and the fourfold Ge^{2+} site on the Ge/SnO_2 cluster model. H_2O was predicted not to stabilize on either of the fourfold sites as well. CH_3O, CH_2O_2, and OH species were predicted to stabilize on both fourfold sites, and the adsorption energies at these sites were calculated. All of the examined oxygenated species and H_2O and OH species were predicted to stabilize on the fivefold Sn^{4+} site. Since CH_3OH and CH_2O were predicted not to stabilize on both the fourfold Sn^{2+} site and the fourfold Ge^{2+} site and the calculated adsorption energies of these C_1-oxygenates were smaller than those of the other examined oxygenated species on the fivefold Sn^{4+} site, we suggested that the produced CH_3OH and CH_2O on both the SnO_2 (110) surface and the Ge/SnO_2 (110) surface easily desorbed in comparison with other CH_3O, CH_2O_2, and OH species.

Table 4
Calculated adsorption energies ADJF (kcal/mol) and net charges NC (|e|) of each adsorbed molecule on the monolayer reduced Ge/SnO_2 and SnO_2 (110) clusters

	Ge/SnO_2 (110)			SnO_2 (110)			
	4-Fold Ge^{2+}			4-Fold Sn^{2+}		5-Fold Sn^{4+}	
	ADE	NC		ADE	NC	ADE	NC
CH_3OH	–	–		–	–	13.4	+0.21
CH_3O	48.1	–	0.16	58.7	−0.33	56.5	−0.18
HCHO	–	–		–	–	18.7	+0.06
CH_2O_2	93.4	−0.43		100	−0.66	95.2	−0.61
OH	64.8	−0.19		76.8	−0.35	73.7	−0.28
H_2O	–	–		–	–	9.8	+0.17

All of the calculated net charges of the chemisorbed hydrocarbon species were predicted to have negative values on every fourfold Ge^{2+} and Sn^{2+} site. On the fivefold Sn^{4+} site, all of the net charges of CH_3OH, CH_2O, and H_2O were predicted to have positive values. The other hydrocarbon species and OH species were predicted to have negative values.

From these simulated properties of the chemisorbed oxygen species on the Ge/SnO_2 (110) surface, we assumed that the smaller amount of chemisorbed oxygen atoms through the reactions and the obstruction of oxygen migration were favorable for an increase of the selectivity of C_1-oxygenates in the direct selective oxidation of methane. The produced HCHO and CH_3OH on the Ge/SnO_2 were predicted to immediately desorb.

4. Conclusions

C_1-oxygenates were obtained over germanium-incorporating SnO_2 ($Sn_{1-x}Ge_xO_2$) in the selective oxidation of methane in the presence of NO. The main product of the C_1-oxygenates was formaldehyde, and its selectivity for $Sn_{0.9}Ge_{0.1}O_2$ gradually increased with temperatures from around 660 K and then decreased rapidly from ca. 810 K. The variation of CH_3OH selectivity was similar to that of HCHO, but its value was smaller. The selectivity for HCHO increased with the content of germanium ion and had a maximum value at $x = 0.2$.

Since we measured a larger proportion of CO_2 selectivity in comparison with CO selectivity in the presence of $Sn_{0.9}Ge_{0.1}O_2$ at 10% CH_4 conversion for the direct selective oxidation of methane, we assumed that the catalyst reactions were dominant in a lower temperature region below ca. 860 K. We suggested that the C_1-oxygenates at 10% CH_4 conversion were produced on the $Sn_{0.9}Ge_{0.1}O_2$ catalyst, not in the gas phase.

The incorporated germanium ions were expected to stabilize at the fourfold Sn^{2+} site on the topmost layer, from the DFT theoretical calculations. This stabilized Ge ion changed the interaction of the O_2 molecule. All of the calculated adsorption energies of the O_2 molecule on the Ge/SnO_2 (110) surface were smaller than those on the SnO_2 (110) surface. We assumed that the coverage of chemisorbed oxygen on the Ge/SnO_2 (110) surface was expected to be smaller than that on the SnO_2 (110) surface through the reactions. Furthermore, we predicted the restriction of oxygen migration to the nearest-neighboring row of the fourfold Sn^{2+} site on the Ge/SnO_2 (110) surface from a quite large value of migration potential. From these simulated properties of the chemisorbed oxygen species on the Ge/SnO_2 (110) surface,

we assumed that the smaller amount of chemisorbed oxygen atoms through the reactions and the obstruction of oxygen migration were favorable for an increase in the selectivity for C_1-oxygenates in the selective oxidation of methane.

Acknowledgments

We acknowledge financial support from the New Energy and Industrial Technology Department Organization (NEDO) and Japan Science Technologies (JST).

References

[1] T.J. Hall, J.S.J. Hargreaves, G.J. Hutchings, R.W. Joyner, S.H. Taylor, Fuel Process. Tech. 42 (1995) 151.
[2] D.M. Newitt, A.E. Huffner, Proc. R. Soc. London, A Math. Phys. Sci. 147 (1934) 555.
[3] R. Pitchai, K. Klier, Catal. Rev. Sci. Eng. 28 (1986) 13.
[4] K. Tabata, Y. Teng, T. Takemoto, E. Suzuki, M.A. Bañares, M.A. Peña, J.L.G. Fierro, Catal. Rev. 44 (2002) 1.
[5] M.A. Bañares, J.H. Cardoso, G.J. Hutchings, J.M.C. Bueno, J.L.G. Fierro, Catal. Lett. 56 (1998) 149.
[6] T. Kobayashi, Catal. Today 71 (2001) 69.
[7] S. Irusta, E.A. Lombardo, E.E. Miró, Catal. Lett. 29 (1994) 339.
[8] K. Otsuka, R. Takahashi, I. Yamanaka, J. Catal. 185 (1999) 182.
[9] K. Tabata, Y. Teng, Y. Yamaguchi, H. Sakurai, E. Suzuki, J. Phys. Chem. 104 (2000).
[10] D.A. Dowden, C.R. Schnell, G.T. Walker, in: Proceedings of the Fourth International Congress on Catalysis, Moscow, 1968, p. 201, Paper 62.
[11] K. Otsuka, M. Hatano, J. Catal. 108 (1987) 252.
[12] J.E. Lyons, P.E. Ellis Jr., V.A. Durante, Stud. Surf. Sci. Catal. 67 (1990) 99.
[13] S.H. Taylor, J.S.H. Hargreaves, G.J. Hutchings, R.W. Joyner, Catal. Today 42 (1998) 217.
[14] G.J. Hutchings, S.H. Taylor, Catal. Today 49 (1999) 105.
[15] C.A. Cooper, C.R. Hammond, G.J. Hutchings, S.H. Taylor, D.J. Willock, K. Tabata, Catal. Today 71 (2001) 3.
[16] H.F. Liu, R.S. Liu, K.Y. Liew, R.E. Johnson, J.H. Lunsford, J. Am. Chem. Soc. 106 (1984) 4117.
[17] Y. Nagasawa, T. Choso, T. Karasuda, S. Shimomura, F. Ouyang, K. Tabata, Y. Yamaguchi, Surf. Sci. 433–435 (1999) 226.
[18] T. Kawabe, K. Tabata, E. Suzuki, Y. Yamaguchi, Y. Nagasawa, J. Phys. Chem. B 105 (2001) 4239.
[19] (a) Y. Yamaguchi, Y. Nagasawa, S. Shimomura, K. Tabata, E. Suzuki, Chem. Phys. Lett. 316 (2000) 477;
(b) Y. Yamaguchi, Y. Nagasawa, K. Tabata, E. Suzuki, J. Phys. Chem. A 106 (2002) 411;
(c) Y. Yamaguchi, K. Tabata, E. Suzuki, Surf. Sci. 526 (2003) 149.
[20] C. Nozaki, K. Tabata, E. Suzuki, J. Solid State Chem. 154 (2000) 579.
[21] B. Delley, J. Chem. Phys. 92 (1990) 508, DMol^3 is provided by Accelrys Inc., San Diego, CA.
[22] A.D. Becke, Phys. Rev. A 38 (1988) 3098;
C. Lee, W. Yang, R.G. Parr, Phys. Rev. B 37 (1988) 785.
[23] V.E. Henrich, P.A. Cox, in: The Surface Science of Metal Oxides, Cambridge University Press, New York, 1994, p. 149.
[24] W. Copel, Prog. Surf. Sci. 20 (1985) 9.
[25] R.W.G. Wyckoff, Crystal Structures, vol. 1, Interscience, New York, 1963.
[26] T. Hahn (Ed.), International Tables for Crystallography, vol. A, Kluwer, Dortrecht, 1995.
[27] T. Kawabe, K. Tabata, E. Suzuki, Y. Ichikawa, Y. Nagasawa, Catal. Today 71 (2001) 21.